INNOVATIONS FOR THE CMS HCAL*

J. FREEMAN

Fermilab, MS 205, Batavia, IL 60510-500, USA
freeman@fnal.ger

The CMS hadron calorimeter (HCAL) is a sampling calorimeter with brass absorber plates and sheets of a scintillator as the active medium.[1] The scintillator is divided into tiles that are optically summed into projective towers. The overall concept of CMS is a large high field magnetic volume instrumented by all-silicon tracking. A very high resolution crystal electromagnetic calorimeter follows the tracker. Finally, the HCAL is stationed at the outer radius of the magnetic volume, just inside the superconducting solenoidal magnet.

One of the tasks before us while designing the CMS HCAL was selection of the front-end signal preparation. The central part of the HCAL uses a photon detector and digitizing electronics. The choice/design of the photon detector and front-end electronics are very tightly tied together. The front-end electronics has to accommodate the sensitivity, capacitance, shaping, and other properties of the photon detector. In the development of the HCAL these two tasks of developing the front-end electronics and the photon detector were done in parallel.

The CMS HCAL consists of four regions. The barrel and endcap HCALs, HB and HE, use a scintillator as the active medium and are located in the central detector. The very forward calorimeter, HF, based on Cerenkov radiating quartz fiber, is located in the forward region outside of the magnetic field volume. The central HCAL sits inside the CMS solenoidal superconducting magnet. The final region — the outer calorimeter HO — sits outside the central magnet and, like the central calorimeters it has a scintillator as the active medium. Figure 1 shows the relative placement of the HB, HE, and HO.

The choice of placement of the HCAL inside the solenoid increases the bending path for the muon system. Additionally, placement of the HCAL immediately adjacent to the electromagnetic calorimeter (as compared to being on the outside
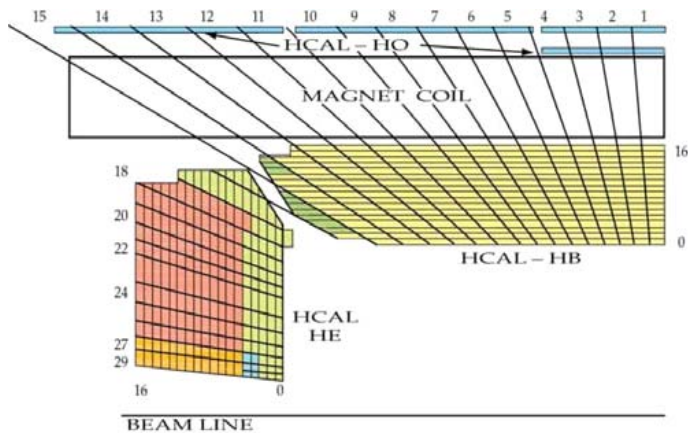
Fig. 1. The relative placement of the central HCAL relative to the solenoid.

of the magnet) allowed for a very conservative robust magnet design. (The solenoid is about one hadron absorption length thick at 90°.)

The CMS central HCAL is a scintillator-based sampling calorimeter. It has thin layers of a scintillator interleaved between brass absorber plates. To maximize the absorber thickness in the small available space (about 1 m radially), the brass plates are relatively thick ($\sim$5.5 cm) and the scintillator is relatively thin (3.8 mm).

Figure 2 shows the layout of the optical design of the calorimeter. Light from the scintillator layers is carried to photodetectors at the back of the calorimeter.
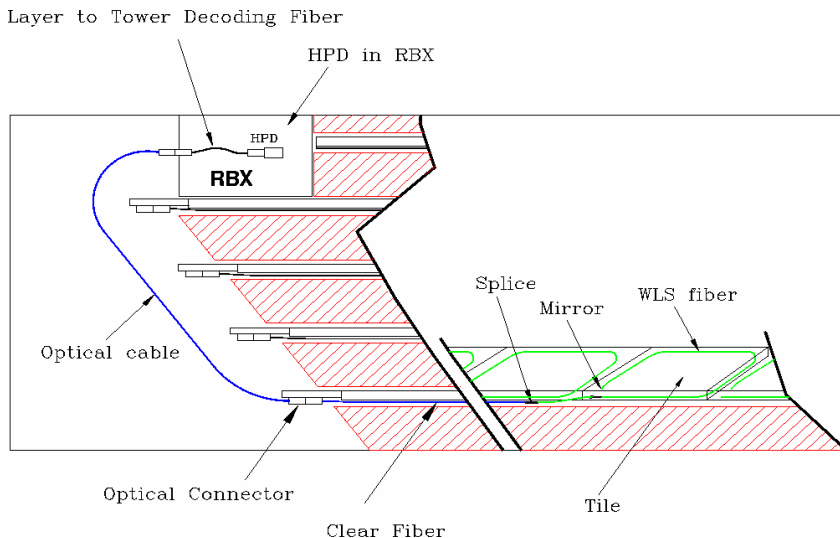

Fig. 2. A schematic view of the CMS HCAL detector. Scintillating tiles are read out with wavelength shifting fibers, which are then coupled to clear fibers. The clear fibers carry the light to the outer radius of the HCAL where photodetectors and front-end electronics are located.

The "art" of developing a detector concept for a new energy regime requires both physics judgment and guesswork as to what the interesting topics will be. Additionally, in the environment of more than one similar detector (as in the case of ATLAS and CMS) there is a wish for the detector to be complementary to the other and have unique abilities. We have seen this in the case of CMS, where electromagnetic calorimeter resolution and muon momentum resolution were emphasized. This concept directed us toward a very large high field magnet, and precise electromagnetic calorimetry. The effect of these choices on the HCAL was that it needed to be placed inside the large, thick solenoid. This caused the HCAL design to focus on high density (and a low active sampling fraction), to be nonmagnetic, and to operate in the 4 tesla field.

A unique feature of CMS is its moving-ring-based structure, allowing for very good access and maintenance of the detector elements. This design feature had the tradeoff for the HCAL in that the readout system (front-end electronics system) had to be placed inside the magnetic volume. Any alternative location for the photodetectors was so far away that there would have been prohibitively large light loss in the long clear optical fibers.

An investigation of possible thin active media that would work in a magnetic field and survive the radiation dose and particle fluxes of the LHC led us to the choice of layers of a scintillator. To read out the optical signal we searched for photodetectors that can operate in a 4 T field. Figure 1 shows the placement of the central barrel and endcap HCALs inside the solenoid magnet. It is interesting to note the relative thickness of the calorimeters compared to the magnet. Tower numbers are indicated. The photodetectors and front-end electronics were placed in small notches at the outer radii at eta tower 14 (HB) and tower 18 (HE).

In the mid-1990s, when we made our search for suitable photodetectors, there were a number of options: photomultipliers, photodiodes, APDs, microchannel plates, and various types of hybrid photodiodes (HPDs). Our desired parameters for the device were:

(1) The device had to work in the 4 T magnetic field.
(2) Our anticipated light yield was 100–300 photons per GeV. We needed a device that had an acceptable quantum efficiency (at least 10%) in the 500 nm region, where our light signal would be.
(3) The front-end electronics noise was anticipated to be around 5000 electrons/ 25 ns sample. We did not want the electronics noise to profoundly degrade the calorimeter resolution, so this placed limits on the minimum acceptable amplification gain of the photodetector.
(4) The spread in variation of amplification of photoelectrons (excess noise factor) should be small enough that it did not seriously affect the calorimeter resolution.
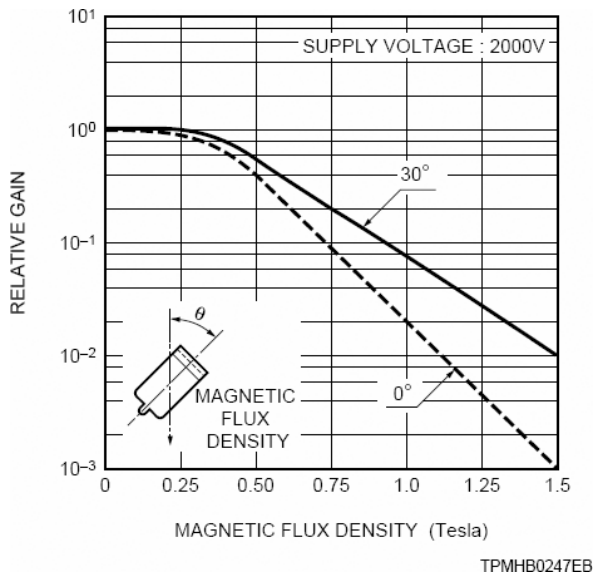(5) The radiation level was anticipated to be ~ 1 Krad and the device had to withstand this.

(6) The device had to have an operating lifetime of 10 years or more.

(7) The device had to be reasonably compact so as to fit in the region allowed for electronics. To fit our desired calorimeter segmentation we wanted the size of the photodetector per channel to be of order 20 cc or less.

(8) The cross-sectional area of the optical fibers that would constitute a calorimeter segment was a circle with a diameter of about 5 mm, so the photodetector had to accommodate this.

(9) A final requirement was that the photodetector should be sensitive to small DC light levels. One of the methods of calibrating the HCAL was to place a small radioactive source by the scintillators. The source generated a DC stream of photons in the scintillator. It was important for the photodetector to be able to measure this current. Accuracy of measuring the current corresponded to accuracy of calibration, and hence a-few-percent accuracy was required. The anticipated light level was about 3×10^7 photons per second at the photo-detector.

Let us discuss a scenario with our parameters to understand their role in the choice of the photodetector. We consider a photomultiplier as the baseline. The ability of a photomultiplier to operate in a 4 T field is very dubious, to say the least. We will return to this point later. A photomultiplier can easily have a quantum efficiency of 10% in the green region, so parameter 2 is acceptable. This would then give us 10 photoelectrons (pe) per GeV of the signal. A typical photomultiplier gain can easily be 50 K, so a single pe signal would be 50 K electrons. The amplifier noise would then contribute at the level of 0.1 pe. With 10 pe/GeV, 0.1 pe is 10 MeV, which would be a completely acceptable noise level. Our design goal was less than 100 MeV.

The excess noise factor as a function of amplification M is defined as $\mathrm{ENF}(M) = 1 + \sigma(M)^2/M^2$. A perfect amplifier with no noise would have $\sigma(M) = 0$, and the excess noise would be 1.0. If this were the case for a photomultiplier, then the single pe would appear as a delta function at 50 K electrons (gain = 50 K). This is in fact not the case for photomultipliers, which typically have an ENF of 1.3. This means that the single pe peak would have a sigma of about 30% or about 15 K electrons (at a central value of 50 K electrons). Since the pedestal sigma of our front-end electronics (centered at 0 electrons) is 5 K electrons wide, the single pe would be very well separated from the pedestal and would be clearly visible. The ability to cleanly see the single pe peak is useful for monitoring gain and performance, and hence would be a very desirable condition.

A typical small photomultiplier tube can have a size of 1 cm diameter and 10 cm length (including the base), for a volume of 8 cc, which fits our desired volume, and the desired active area for the fiber bundle. Most choices of phototube window will survive 1 Krad with no degradation.

So we conclude that a phototube would be a very satisfactory choice for our photodetector, with the proviso that it should work in a 4 T field. Unfortunately,

Fig. 3. Reduction in gain of a photomultiplier tube vs. magnetic field strength (Hamamatsu high magnetic field fine mesh phototube R6504).

phototubes lose their gain quickly in a magnetic field (due to inability to focus the electrons). Figure 3 shows the gain loss vs. magnetic field for a typical phototube. A survey of different structure phototubes yielded no candidate that could operate in fields much above 1 T.

Table 1 shows photodetectors available during the mid-1990s, with the exception of SIPMs, which are a recent development. The "Bias voltage" row indicates typical operating voltages. The Photon lifetime row displays the lifetime number of photons a typical device (under normal gain conditions) can survive. The "Expected electrons per GeV" row shows the number of electrons per GeV the HCAL would expect, folding in the device's gain and quantum efficiency.

Looking at Table 1, we can immediately eliminate photodiodes (PDs) from consideration. Although they have many desirable features, the unity gain implies that our electronics noise level of 5000 e^- would correspond to a $50\,\text{GeV}$ signal.

Microchannel plates (MCPs) have a long history. Until recently they had a very limited charge lifetime. Additionally, until recently the large channel diameter limited their operational magnetic field limit to about 1–$1.5\,\text{T}$. At the time of our decision (and even now) they were unsuitable due to the limited lifetime and magnetic field performance. (In the ensuing $10+$ years since our evaluation of photodetectors, some devices, particularly MCPs, have improved their properties. Current MCPs can have a charge lifetime of up to $0.1\,\text{C}$ and demonstrated operation in $2\,\text{T}$ magnetic fields.)

As mentioned earlier, photomultipliers (PMTs) cannot operate in the $4\,\text{T}$ magnetic field.

Table 1. A summary of key properties of photodetectors.

	Requirement	PD	APD	PMT	MCP	HPD	SIPM
Bias voltage (V_b)		>20 V	400 V	1–2 kV	1–5 kV	10 kV	50 V
Timing	1–3 ns	3 ns	3 ns	100 ps	50 ps	100 ps	30 ps
Sensitivity		100 pe	10 pe	1 pe	1 pe	1 pe	1 pe
Quantum efficiency	>10%	40%	80%	20%	20%	20%	30%
Expected e/GeV	>10^4	100	5000	10^6	10^5	2×10^4	3×10^5
Excess noise factor	<1.5	1	2.5–5	1.4	1.2	1.05	1.2
Dynamic range	10^4	>10^7	10^7	10^6	10^3	10^7	10^3–10^4
Gain (M)	>100	1	50–100	10^5–10^6	10^4–10^6	2×10^3	5×10^4–10^6
$\delta V_b/V_b$ for $\delta M/M = 1\%$	5×10^{-4}	—	5×10^{-4}	5×10^{-4}	5×10^{-4}	5×10^{-3}	10^{-3}
δT for $dM/M = 1\%$	1°C	10°C	0.3°C	3°C	3°C	3.5°C	0.3°C
Max magnetic field	>4 T	>4 T	>4 T	~1 T	~1 T	>4 T	>4 T
Radiation tolerance	2 Krad	1 Mrad	1 Mrad	10 Krad	10 Krad		
(rad/n)	10^{11} n	10^{14} n	10^{13} n	10^{14} n	10^{14} n	10^{11} n	10^{13} n
Volume/channel	<20 cc	<1 cc	<1 cc	10 cc	1 cc	10 cc	<1 cc
Photon lifetime	5×10^{16}	No limit	No limit	10^{19}	>10^{11}	10^{17}	>10^{16}

Silicon photomultipliers (SIPMs) are a comparatively recent development and have come into their own as realistic photodetectors only in the last few years. They did not exist in practical form in the mid-1990s. They are included in the table because they will have importance in future HCAL developments, as discussed below.

By elimination we were left with APDs and HPDs. Both of these were considered seriously. APDs have a marginal gain causing the lowest measurable signal to be of order 1 GeV. This would be an unacceptable feature if left alone. However, we speculated that perhaps some electronics developments could reduce the noise level, or perhaps we could operate at a higher gain. When operating at a gain of 50, APDs have a temperature dependence of gain of about 3% per °C. Therefore operating a detector with APDs would require a temperature stability of about 1°C to satisfy our desired energy resolution constant term.

We studied both of the APD and HPD options extensively in the laboratory. We also built prototype HCALs using these two photodetectors and operated them in test beams. Figure 4 shows the test beam results for muons passing through the
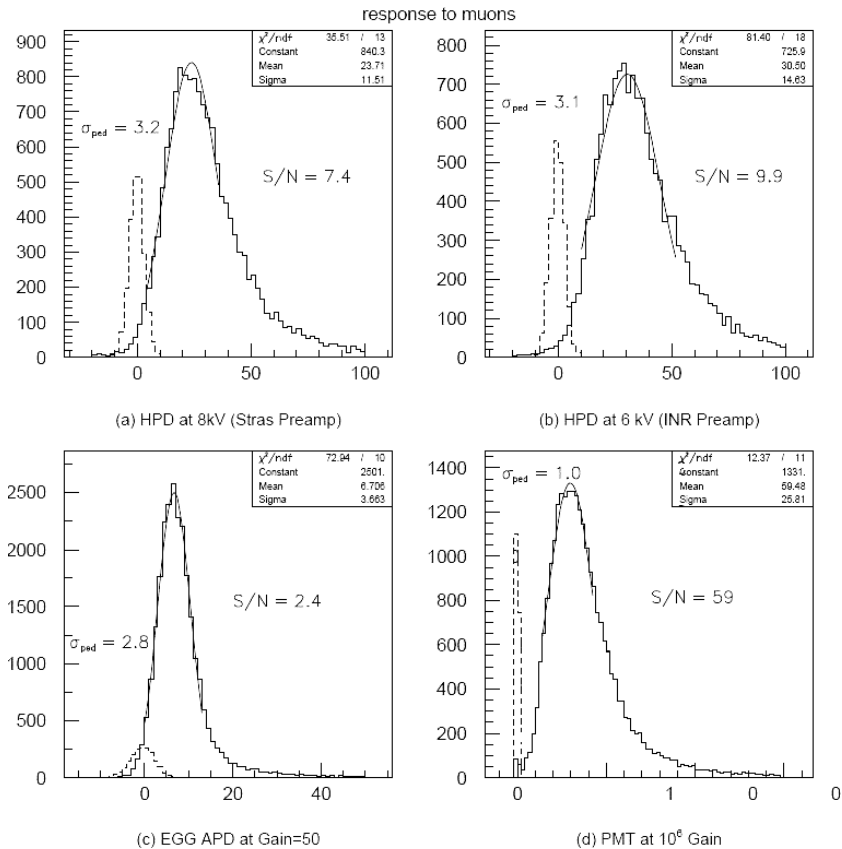

Fig. 4. Test beam comparison of APD vs. HPD vs. PMT for muon response.[2]
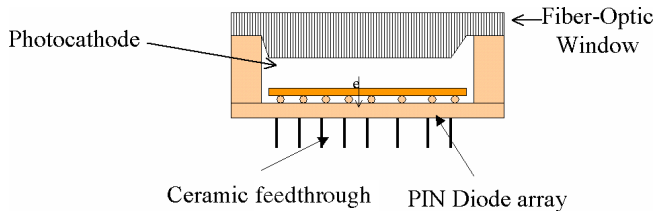
Fig. 5. Cross section of the HPD.

prototype calorimeter. The pedestal and the calorimeter muon response are shown for two types of HPDs (a, b), an APD (c), and a PMT (d). The signal-to-noise ratio S/N is shown for each case. The PMT has an outstanding value of S/N and if not for the magnetic field would have been a good choice. (In fact PMTs were chosen for the readout of the HF detector, which is not situated in a high magnetic field region.) Compared with the APD, the HPDs both show about $3\times$ better S/N due to their higher gain and smaller excess noise factor. It is also worth noting that in this study an amplifier with an unrealistically low bandwidth was used for the APD. This caused the electronics noise to be about 1200 e$^-$, rather than our expected 5000. Use of a realistic amplifier (with a suitable bandwidth for the 25 ns bunch spacing of the LHC) would have resulted in substantially worse S/N for the APD. Finally, the APD required very good temperature stabilization. The combination of these issues led us to choose the HPD as the HCAL photodetector.

Figure 5 shows the cross section of the HPD. It is a vacuum device like the PMT. It has a transparent window followed by a photocathode that absorbs photons and emits photoelectrons. A high voltage ($\sim$10 kV) separates the photocathode from the $\sim$3 mm distant reverse-biased silicon diode. The kinetic energy of the accelerated photoelectrons ionizes the silicon and creates electron–hole pairs (3.6 eV/pair) which are the source of the gain of the device.

Having made the choice of HPD, we were still faced with some R&D to develop the device we wanted for the HCAL.[3] One key requirement was to have a multipixel device to reduce both the required photodetector volume and cost. The silicon diode was segmented into pixels, and the readout signals were carried through ceramic feedthroughs. The silicon diode was thinned from an initial 300 microns to 200 microns to speed the signal.

We observed the presence of capacitive crosstalk between neighboring pixels, which was traced to poor connection between the pixels and the diode bias supply.[4] We specified a layer of aluminization on the front of the diode and aluminization of the sides to carry the back-supplied bias voltage better to the individual pixels. This change eliminated the electrical crosstalk.

To prevent light from spreading into neighboring pixels when transiting the photocathode window, we specified that the window be made of fiber-optic glass. Photocathodes typical of phototubes and the HPD are semitransparent. Some of the light will transmit through the photocathode without interacting, and then
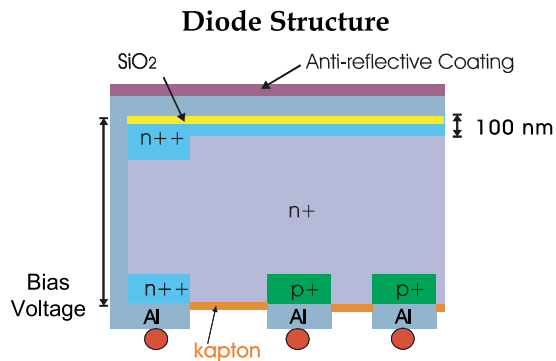
Fig. 6.   An HPD cut in half.

Diode Structure

Fig. 7.   A diagram of the cross section of the HPD silicon diode. Aluminization is shown in gray. A SiO_2 layer prevents contamination of the silicon by the aluminum but allows high frequency coupling of the bias supply to the diode, eliminating the electrical crosstalk. A higher impedance path provides DC coupling of the diode to the bias supply.

hit the silicon diode. This light could reflect back to the photocathode and cause emission of additional photoelectrons. We found that this reflection caused crosstalk between neighboring pixels at the few-percent level. The vendor (DEP, Holland) was asked to develop an antireflective coating optimized for our light spectrum. A cross section diagram of the final diode is shown in Fig. 7.

Before starting mass production of the HPDs, we performed extensive tests. The tests included:

- Radiation damage studies, where we exposed them to 10^{11} neutrons/cm^2 and 15 Krad.
- Magnetic field tests, where the devices were operated in 5 T fields. We also constructed a front-end electronics box, as would be placed on the calorimeter, and tested it in a 3.3 T magnetic field.

- Aging tests, where we measured any changes in performance for integrated charge of up to 10 C corresponding to our 10-year lifetime requirement.
- Test beam studies, to confirm the expected performance.

A total of about 600 HPDs were manufactured and passed our acceptance tests. The devices are working well in CMS central HCALs. As pointed out earlier, conventional photomultipliers were chosen for the HF.

Recently a new device, the SIPM, has become available.[5,6] It is an array of very small Geiger mode APDs in a single package. Typical array densities are 1000–10,000 per mm.[2] These devices offer substantial advantages over the HPDs in that: they are much smaller, allowing finer calorimeter segmentation than was possible for the HPDs; they have substantially higher gain, reducing the noise floor of the calorimeter; and they operate at voltages of order 50 V, much smaller than the 10 KV of the HPDs. This last factor points toward less maintenance issues in the future. Important properties of the SIPM are included in Table 1. The CMS HCAL team is actively pursuing this possibility for future improvements.[7] To study possible upgrades we have installed 144 SIPMs in the HO calorimeter. As expected, their performance is very good. Figure 8 shows the energy distribution for cosmic rays in one HO tower read out with an SIPM. The energy deposition by the muon is cleanly separated from the pedestal.

Front-End Electronics

As we developed the choice of HPD for the HCAL photodetector, we also developed the requirements for the front-end ADC. Some of the requirements were driven by the environment which the electronics would be in, some by the physics goals of our detector, and some by constraints or properties of the HPD.
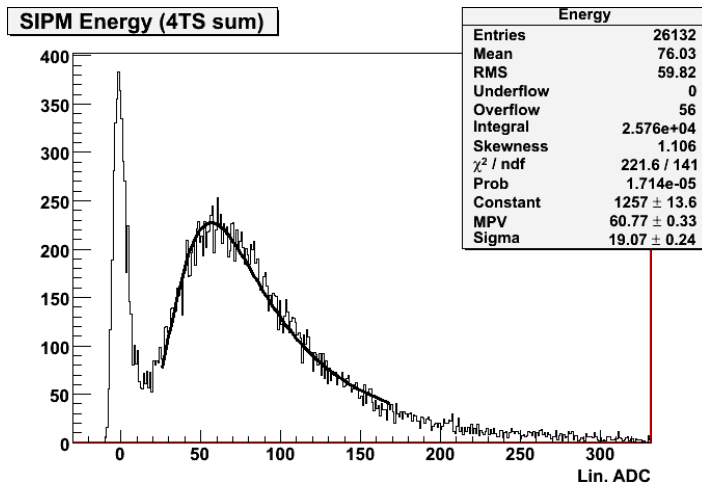

Fig. 8.   Cosmic ray energy pulse height distribution for a CMS HO tower read out with an SIPM.

The electronics was to be placed close to the HPD on the back of the calorimeter. This choice of placement implied that the electronics needed reliability, low power, and radiation tolerance.[8]

The signals from the scintillator have a rise time of about 10 ns and a fall time of about 30 ns. Because the LHC will have high luminosities and large physics occupancy, we desired that the electronics would react to the signal as quickly as possible. The LHC operates at 40 MHz (25 ns buckets) and we wanted the signal to be in as few buckets as possible.

We designed and built a flash ADC (FADC) exactly tailored for the HCAL. We chose to make a totally custom FADC, because of the unique requirements we had in the detector. The FADC we developed is the QIE8 (charge Integrator and Encoder), the eighth generation of a successful FADC that has been developed and used at Fermilab.[9]

For small energy depositions into the calorimeter, the signal shape is not very regular. For this reason we felt that integrating the charge of the signal, rather than measuring a voltage, would give us the best performance. Because the signal for low energies was small, we wanted to have as quiet an amplifier as possible, with a target of a few thousand electrons. With a signal of about 10–20 photoelectrons per GeV and the HPD gain of 2000 (corresponding to 3–6 fC/GeV), we desired a sensitivity of about 1 fC (6000 electrons) and a noise level (pedestal width) of the same order. With the 1 fC minimum, we looked at physics simulations to find the maximum realistic energy deposit per channel. We found that for the 7-on-7 TeV LHC collider, a maximum energy per channel of 3 TeV was adequate. This corresponded to about 10,000 fC. Thus we specified the maximum scale of 10,000 fC and a dynamic range of 10^4.

A conventional linear ADC would require 13+ bits to supply the required dynamic range. Taking into account the typical differential nonlinearities of an ADC, we would need 14 bits of resolution. Because the LHC operates at 40 MHZ, the ADC would also have to sample at 40 MHz. The power required for this size of the flash ADC would be large. Another important consideration in our concept was to minimize the number of bits of information sent off detector to the counting house. (The available volume for the readout fibers was very limited.)

A standard trick to reduce the required size of the flash ADC, and at the same time reduce the amount of data sent off detector, is to put a multirange amplifier in front of the FADC, with each range having a different amplification factor. The signal from each range is sent to circuitry to detect the proper range. The signal from the lowest nonsaturating range is then sent on to the FADC for digitizing. The output data are then the result of the FADC, plus the selected range. Logically one can think of this compound number as the mantissa and exponent of a floating point number. By appropriate choice of the number of ranges, their amplification factors, and the number of bits of resolution of the FADC, the dynamic range can be satisfied and have a large reduction in the number of bits sent off detector.
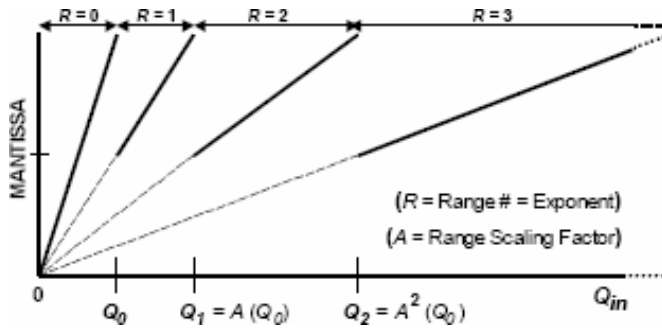
Fig. 9. An example of a four-traditional-range FADC.[9]

Figure 9 shows an example of a typical four-range amplifier/FADC. Each range starts at zero and has a full scale of A^n, with n the range, 0, 1, 2, or 3. A is the gain of the amplifier, and for this example the gain for each range is A times the range of the preceding one. The input charge is on the horizontal scale and the output mantissa is on the vertical scale. The dotted lines indicate unused codes. For example, an input charge of $1.5\,AQ_0$ would generate an output code in range 2. The redundant possible code from range 3 would not be used, because it would have coarser resolution. The result of an algorithm such as this is that there would be many unused codes in order to cover the required dynamic range. This means that more bits are needed to get the required resolution and more data have to be sent off detector.

In Fig. 10 we see an improved design. Here each range does not start from 0 but rather from an offset that is (a little less than) the full scale of the range before it. In this design there are no wasted codes and one gets the highest resolution possible for the number of bits allocated to the FADC. (We note that to avoid having values of charge that generate no code we require a small overlap between the ranges and hence generate a few unused codes.) This is the design we chose for the QIE.
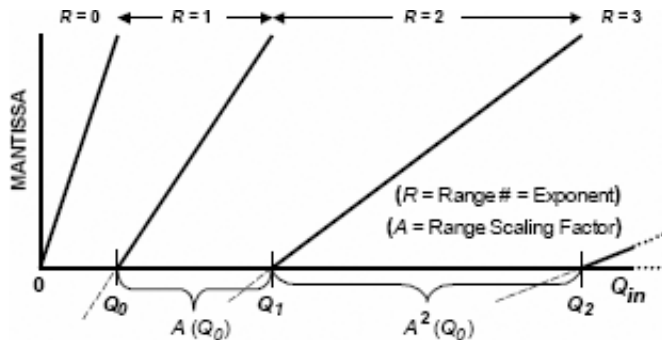

Fig. 10. A four-range FADC where each range has an offset of the maximum scale of the range before it.[9]
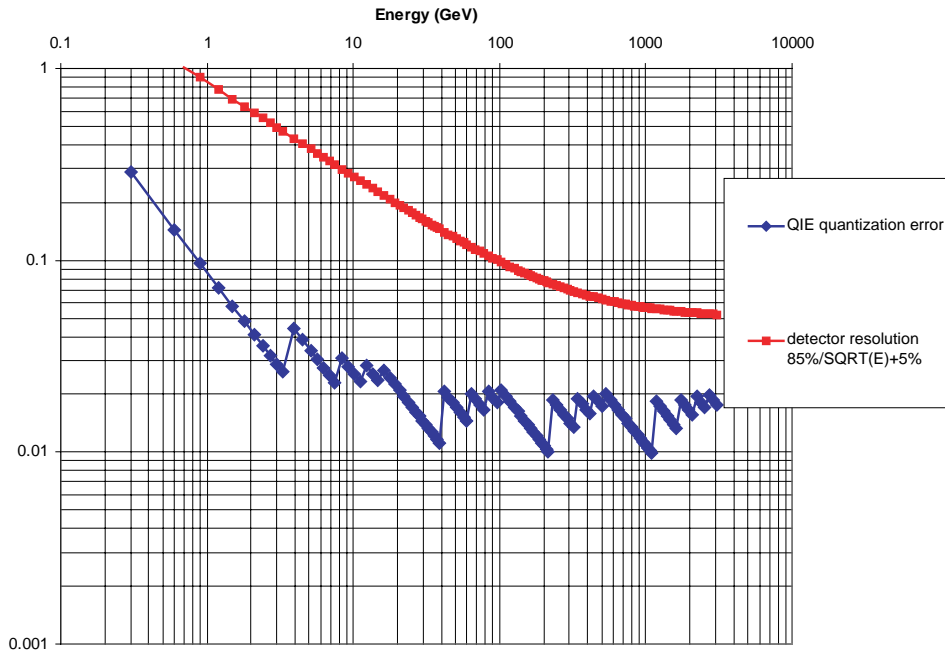
Fig. 11.   The HCAL resolution as a function of energy, and the FADC resolution as a function of energy. The choice of the FADC ladder is shown in the figure heading.[1]

The energy resolution of the HCAL has been measured to be about 85%/ sqrt(E) + 5% for isolated pions. This energy resolution is shown as the smooth curve in Fig. 11, as a function of the energy. A required feature of our FADC was that it not should contribute significantly to the overall energy resolution of the calorimeter. The effect of the finite bin width must then lie significantly below the smooth curve in Fig. 11.

An FADC works by having a ladder of resistors and a voltage comparator at each point along the ladder, comparing the input voltage and the voltage of the point on the ladder. An encoder then senses which is the (for example) highest voltage comparator still less than the input signal. A conventional (linear) FADC ladder has the same value of the resistor all along the ladder. Therefore it has the same voltage drop between comparator ladder points and thus the same bin width for all bins. However, nothing requires that the same resistance value be used everywhere on the ladder. We tailored our ladder (and hence the bin values of the FADC) very carefully to reduce to a minimum the number of bits of resolution needed and at the same time keep the bin width contribution to a resolution well below the native energy resolution of the calorimeter.

Our development led to an FADC with four ranges (*1, *5, *25, and *125) and five bits of (a very nonlinear) ADC. Figure 11 displays the details of the choices. The figure heading shows the selected bins and ranges. We see that the dynamic range requirement of 10^4 is satisfied.

We also satisfied our requirement that the FADC bin width not contribute to the energy resolution. The jagged curve in Fig. 11 shows the bin width of our choice of the FADC ladder and the gain of the four ranges. Looking carefully, one can see that the bin width pattern repeats itself four times. The 5% calorimeter resolution constant term means that at very high energies the energy resolution will asymptotically approach 5%. We see that at very high energies the FADC bin width contribution is about 2%. Added in quadrature with the constant term the binning causes about a 6% worsening of the ultimate calorimeter energy resolution.

To satisfy our dynamic range requirement the design needed 5 bits of the ADC value and 2 bits of the range value, for a total of bits 7. This is about half the number of bits we would have expected from a single range linear FADC. The number of comparators doubles for each bit of the FADC resolution. In the QIE8 design there are 31 comparators; in the 14-bit FADC there would be 16,000.

A final aspect of the design was drawn from our desire to measure radioactive source currents as a means of calibration. As mentioned earlier, the presence of the radioactive source caused the scintillator to generate about 3×10^7 photons per second at the HPD. After the HDP quantum efficiency and gain, this corresponded to about 1 nA or about 150 electrons per 25 ns bucket. We wanted to measure this level accurately because it was a primary means of monitoring the gain of the calorimeter. A 5% error in measuring the radioactive source current would then correspond to a 5% error in the energy scale of the detector. To reach this accuracy we designed the QIE to have a high sensitivity calibration mode. In this mode of operation, the resistors in the ladder were three times higher in value than the nominal ones and all were the same value. In this mode the QIE acted as a linear FADC with 0.3 fC per bin. A control bit allowed us to switch from regular to calibration mode. To perform radioactive source calibrations, we read out the FADC repeatedly and formed histograms with 65,000 entries. We then calculated the mean of the histogram. Figure 12 shows the mean value of the histograms as a function of time. In the middle of the measurement the source was removed. Each dot corresponds to the mean value of the 65,000-entry histogram. Using this technique (of massive oversampling) we were able to measure shifts of the mean by as small as a few 1/1000s of a bin. This gave us the accuracy required for the radioactive source calibration.

The QIE is a four-stage pipelined device that runs at 40 MHz. The four range (approximately 100 MHz bandwidth) preamplifier is constantly at work, amplifying the input signal. At pipeline stage 1, integrators for the four ranges integrate the charge in a 25 ns gate; at stage 2, the lowest range that is not full-scale is selected, and the voltage presented to the FADC; at stage 3 the FADC digitizes the voltage; at the final stage, stage 4, the capacitor is reset; and then back to stage 1. In the
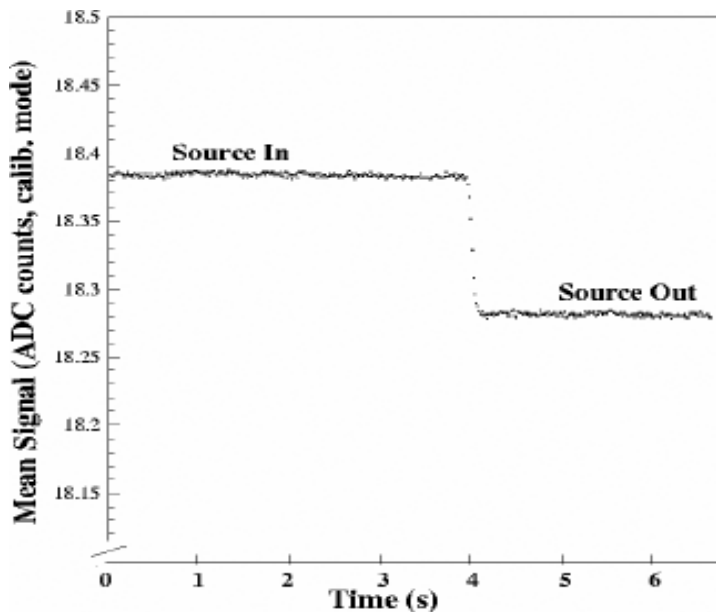
Fig. 12.   The mean ADC value in calibration mode for the source in position by the scintillator, and out. The source caused about a 0.1 bin shift, corresponding to about 200 e$^-$/25 ns.[9]

QIE there are four independent capacitors, each at a different stage of the four-stage cycle. Thus every 25 ns a new 5-bit + 2-bit number is generated.

The penalty for the novel arrangement of the QIE amplifier gains and offsets is an abundance of calibration constants. Each of the four capacitors in the "round robin" can (and does) have slightly different constants. There are four ranges with slope and offset for a total of 32 calibration constants. Additionally, there can be variation in the ladder that can be measured. About 18,000 QIE chips were calibrated and tested in an automated robotic testing station. The robot sorted the chips based on test results. After the good chips were mounted on electronics boards, they were given a final, detailed test. An example of a test result, the slope for the set of chips for one of the ranges, is shown in Fig. 13.

Summary

The CMS HCAL photodetector and front-end electronics were developed simultaneously. The high magnetic field where the HCAL is located caused a severe limitation on the choice of photodetector. In fact no suitable photodetector existed and we were forced to develop our own, a pixilated proximity-focused HPD. The low gain of the HPD (1000–2000) and the limited light yield of the sampling scintillator calorimeter (10–20 pe/GeV) necessitated the development of a very sensitive and low noise front-end readout. We developed a novel range-switching nonlinear FADC, the QIE8, for this purpose. It has a sensitivity of 1 fC and a noise level of
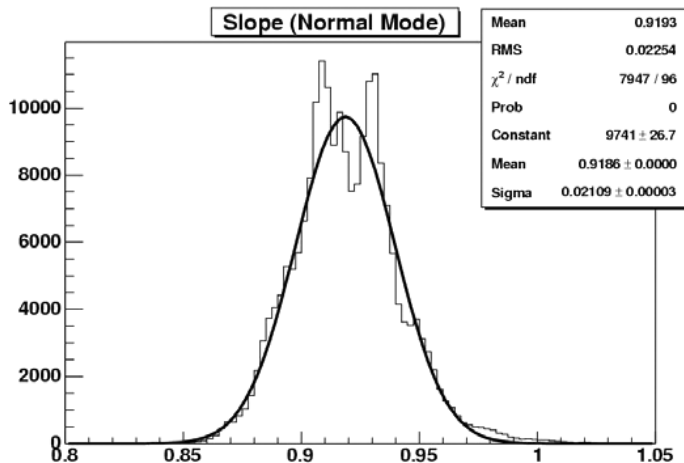
Fig. 13.   Slope measurement for a set of QIE chips for one of the four ranges.[10]

about 0.7 fC. The required 10,000–1 dynamic range was achieved using a very non-linear response function of the 5-bit FADC and automatic switching between four ranges of preamplifier gain. The readout of the calorimeter channel requires only 7 bits of data rather than 14 bits for a completely linear single range readout. The data compression reduces front-end power requirements and minimizes the cable volume leaving the detector.

References

1. CMS Collab., *J. Instrum.* **3**, S08004v (2008).
2. P. B. Cushman, *Nucl. Instrum. Methods A* **387**, 107 (1997).
3. P. B. Cushman and A. H. Heering, *IEEE Trans. Nucl. Sci.* **49**, 963 (2002).
4. P. Cushman, A. H. Heering, N. Pearson, J. Elias, J. Freeman, D. Green and A. Ronzhin, *Nucl. Instrum. Methods A* **504**, 62 (2003).
5. Z. Sadygov *et al.*, *Nucl. Instrum. Methods A* **567**, 70 (2005).
6. B. Dolgoshein *et al.*, *Nucl. Instrum. Methods A* **567**, 70 (2005).
7. A. Heering *et al.*, *Nucl. Instrum. Methods A* **576**, 341 (2007).
8. T. M. Shaw *et al.*, Front end readout electronics for the CMS hadron calorimeter, in *IEEE 2002 NSS*, Norfolk, Virginia, USA, 10–16 Nov 2002.
9. T. Zimmerman and J. R. Hoff, *IEEE J. Solid State Circuits* **39**, 895 (2004).
10. E. Hazen *et al.*, *Nucl. Instrum. Methods A* **511**, 311 (2003).
11. J. Damgov *et al.*, HB performance and validation of calibrations using CRAFT, and LHC beam data of September 2008, CMS Note 2009/999, May 24, 2009.